Carving entangled multiparticle states with exponentially improved fidelity

Joshua Ramette, Josiah Sinclair, Zeyang Li,* and Vladan Vuletić
Department of Physics, MIT-Harvard Center for Ultracold Atoms and Research Laboratory of Electronics, Massachusetts Institute of Technology, Cambridge, Massachusetts 02139, USA

(Received 29 January 2024; revised 19 March 2025; accepted 25 March 2025; published 14 May 2025)

We propose a method that uses the "no-jump" evolution of a probe to generate entangled multiparticle states of high fidelity. The probe is coupled to a target ensemble of qubits and engineered to exponentially decay at a rate depending on the target collective spin, such that postselecting on observing no probe decay precisely removes select faster-decaying spin components. When a probe and N-qubit target interact via a cavity mode of cooperativity C, our procedure generates entangled states with infidelities of $e^{-C/N}$, an exponential improvement over previous carving schemes. This scheme, which we call "counterfactual" carving, can generate complex entangled states for applications in quantum metrology and quantum computing.

DOI: 10.1103/PhysRevA.111.052426

I. INTRODUCTION

Entangled multiparticle quantum states represent a valuable resource, enabling measurements beyond the standard quantum limit, secure communication networks, and quantum computation [1–12], with the fidelity of the generated entanglement of primary importance for many of the most impactful applications [13–15]. To generate an entangled state starting from an easily prepared product state of many qubits, one can either apply a deterministic unitary operation [16–18] or attempt to alter the state vector via a projective measurement onto a subspace of interest [19].

The interaction between an ensemble of N qubits and a cavity mode is a well-explored and promising way to generate entanglement. While certain symmetry considerations allow, in principle, the perfect generation of two-body entanglement [11,20], known methods for generating entanglement using cavity QED interactions for multiparticle systems of N qubits are fundamentally limited by loss mechanisms characterized by the cavity cooperativity C. Previous approaches such as [16–18,20–24], whether employing deterministic techniques or postselection, are all limited by the finite atom-cavity coupling strength relative to photon losses, leading to infidelity scalings no better than $1/C$, with some methods also having absolute infidelity floors [17,18].

One of the best performing classes of these methods for preparing a highly entangled state involves "carving" out certain collective spin components (Dicke states [25]) $|m\rangle$ via a cavity measurement (see [21,22] for proposals and [23,24,26] for experimental realizations). For these methods, the detection of a multifrequency photon transmitted through an optical cavity projects the spin system into an entangled superposition of Dicke states, $\sum c_m |m\rangle$. We call these approaches "factual" carving since postselection occurs on the detection of a transmitted probe photon, which is correlated with the occupation of certain Dicke states of the ensemble. For factual carving, the infidelity ϵ_f of the carved state scales as $\epsilon_\mathrm{f} \sim (C/N)^{-1}$, where C is the cavity cooperativity, characterizing the coupling of a single atom to a single intracavity photon. The infidelity ϵ_f is caused by the spectral overlap of the atom-shifted cavity resonances (i.e., different Dicke states) [21,27] being polynomially large in C/N.

In this work, we propose an alternative kind of carving method which yields infidelity scaling as $e^{-C/N}$, an exponential improvement compared to all existing schemes for generating multiparticle entanglement. We call this scheme "counterfactual" carving because the generation of entanglement is heralded by the absence of evolution ("no quantum jump" [28,29]) of a probe coupled to the atomic ensemble. The improved scaling arises from engineering an exponential decay which carves away particular spin components. This method enables the generation of large highly entangled states, for example, superpositions of Dicke states or N-atom Greenberger-Horne-Zeilinger (GHZ) states [30–32], that are useful for many quantum applications [7,14,33,34].

II. ATOM-CAVITY COUPLING HAMILTONIAN

To demonstrate the principles of counterfactual carving and directly relate it to the most pertinent prior works, we consider a setup similar to [21,22] and shown in Fig. 1, consisting of an ensemble of N target atoms coupled to a cavity mode, with the addition of a photon source atom s that we use to probe the target. The internal structure of each atom constitutes a Λ system where two ground states $|\uparrow\rangle, |\downarrow\rangle$ are coupled to an excited state $|e\rangle$, and for simplicity we assume that $|e\rangle$ decays predominantly to the ground state $|\uparrow\rangle$ and is only weakly coupled to $|\downarrow\rangle$. The optical transition $|\uparrow\rangle \rightarrow |e\rangle$ of frequency ω_e and population decay rate Γ_e is coupled to the cavity mode $\hat{a}$ of frequency ω_c with single-atom Rabi frequency $2g$ and population decay rate $\kappa \ll \Gamma_e$ with a large

*Present address: Department of Applied Physics, Stanford University, Stanford, California 94305, USA.

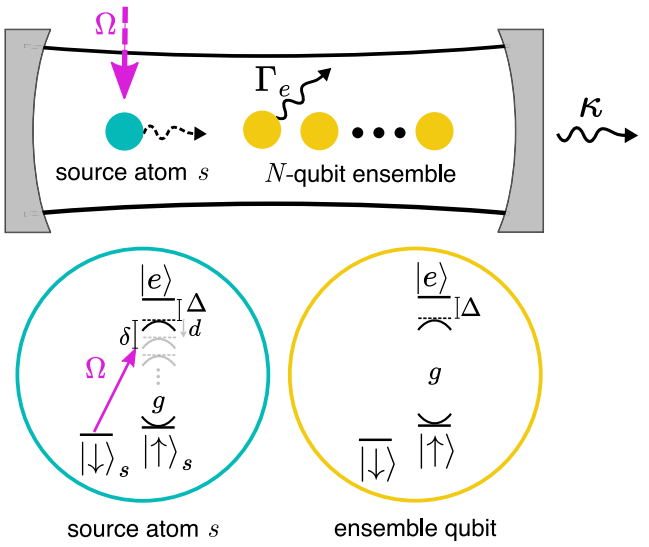

FIG. 1. Counterfactual carving of a qubit ensemble (target) using an optical cavity. The cavity contains N qubits (yellow) and a single-photon source atom s (teal). As shown in faded gray on the source-atom level scheme, each ensemble atom coupled to the cavity mode (in $|\uparrow\rangle$) shifts the cavity resonance frequency by d. A transverse laser beam Ω (purple) addresses s and can be frequency tuned so that the emission on the Raman transition $|\downarrow\rangle_s \to |e\rangle \to |\downarrow\rangle_s$ in the source atom is tuned to near the frequency-shifted cavity resonance. The absence of emission into the cavity, as detectable via the state of the source atom, modifies the target collective state.

detuning $\Delta \equiv \omega_e - \omega_c$, with cooperativity $2C \equiv 2g^2/(\kappa\Gamma_e)$ [35].

The interaction of the target ensemble with the cavity mode is governed by the Hamiltonian

$$H_{\text{target}} = -\Delta\hat{a}^\dagger\hat{a} + g\hat{a}\sum_{i=1}^{N}|e\rangle_i\langle\uparrow| + \text{H.c.}$$
$$= -\Delta\hat{a}^\dagger\hat{a} + g\hat{a}\sum_{m=0}^{N}\sqrt{m}\,|m_e\rangle\langle m| + \text{H.c.}, \qquad (1)$$

where we have reexpressed the Hamiltonian as acting on the collective spin states $|m\rangle$ ($|m\rangle$ is the symmetric state with m atoms in $|\uparrow\rangle$ and $N-m$ atoms in $|\downarrow\rangle$). $|m_e\rangle$ represents the state where $|m\rangle$ has collectively absorbed a photon from the cavity (see the Supplemental Material [36]). This Hamiltonian couples the state $|1\rangle_c|m\rangle$ to $|0\rangle_c|m_e\rangle$ with coupling strength $\sqrt{m}g$ and a detuning of Δ, shifting the frequency of $|1\rangle_c|m\rangle$ by $md \equiv mg^2/\Delta$ in the dispersive limit $g \ll \Delta$, where assuming $\kappa \ll \Gamma_e$, it is favorable to be far detuned from the excited state. Here, $|p\rangle_c$, with $p = 0, 1$ denoting the cavity state with p photons. For sufficiently large single-atom cooperativity C, each of these Dicke states, with m atoms in $|\uparrow\rangle$, corresponds to a spectrally resolved Lorentzian line, as in Fig. 2(a).

III. PROBING CAVITY RESONANCES TO CARVE DICKE STATES

To probe the m-dependent energy shifts and counterfactually carve the desired superposition of Dicke states $|m\rangle$,

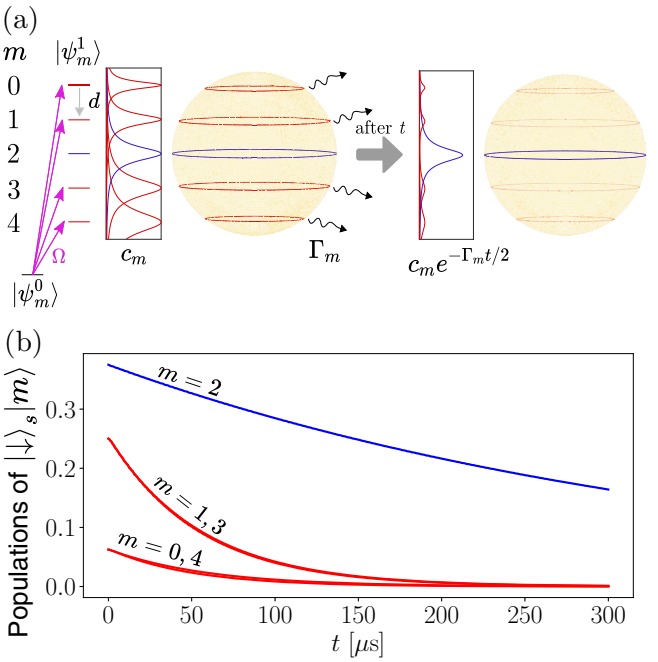

FIG. 2. Preparation of the $|m = 2\rangle$ Dicke state by counterfactual carving from a CSS $\propto (|\uparrow\rangle + |\downarrow\rangle)^{\otimes 4}$ of $N = 4$ atoms. Resonantly addressed levels (red) decay quickly, and the unaddressed level (blue), driven only off resonantly, decays more slowly. After time t, the populations of the undesired components are exponentially suppressed. (a) The ensemble-cavity coupling shifts the frequency of the cavity mode of width κ by md. A tone of Ω driving s induces a coupling $w = \Omega g/\Delta$ between dressed states $|\psi_m^0\rangle$ and $|\psi_m^1\rangle$. (b) Numerical simulation of the master equation for the no-jump evolution of the joint source-target system, showing the remaining populations of $|\downarrow\rangle_s|m\rangle$. Parameters used were $\kappa = 2\pi \times 0.2$ MHz, $\Gamma_e = 2\pi \times 6$ MHz, $g = 2\pi \times 8.5$ MHz, with $C = 60$, $\Delta = \sqrt{2}g\sqrt{\Gamma_e/\kappa} = 2\pi \times 66$ MHz.

we use the separately addressable atom s, which acts as a single-photon "source." (For another use of such a source atom, see [20].) We initialize s in $|\downarrow\rangle_s$, then couple it to $|e\rangle_s$ with a laser beam of strength Ω and detuning δ relative to the empty-cavity resonance. For simplicity, we take the coupling Ω to be much smaller than all other energy scales in the problem. The Hamiltonian for s is the same as for the target atoms, but with the additional laser coupling Ω,

$$H_s = -(\Delta + \delta)\,|\downarrow\rangle_{s\,s}\langle\downarrow|$$
$$+ \Omega\,|e\rangle_{s\,s}\langle\downarrow| + g\hat{a}\,|e\rangle_{s\,s}\langle\uparrow| + \text{H.c.} \qquad (2)$$

Here the subscript s indicates the source atom, and the total Hamiltonian is $H_{\text{tot}} = H_{\text{target}} + H_s$.

As Fig. 1 illustrates, tuning δ into resonance with the cavity shifted by a particular Dicke state $|m\rangle$ then enables s to emit a photon into the cavity via the Raman transition, $|\downarrow\rangle_s \to |e\rangle_s \to |\uparrow\rangle_s$. The photon subsequently leaves the cavity at rate κ. In this way, the (potential) decay of the source atom ($|\downarrow\rangle_s \to |\uparrow\rangle_s$) via the cavity reveals the occupation of the corresponding ensemble Dicke state $|m\rangle$. If the source atom is observed to have not decayed for a time that is long compared to the characteristic decay time via this channel, then the corresponding amplitude of $|m\rangle$ is exponentially suppressed,

as in Fig. 2(b). To annihilate the amplitudes of more than one Dicke state, multiple tones Ω can be used, as in Fig. 2(a).

Diagonalizing $H_{\rm tot}$ to first order with respect to the atom-cavity coupling, we obtain the dressed states $|\psi_m^0\rangle \equiv |0\rangle_c |\downarrow\rangle_s |m\rangle$ and $|\psi_m^1\rangle \equiv |1\rangle_c |\uparrow\rangle_s |m\rangle - \frac{g}{\Delta} |0\rangle_c (|e\rangle_s |m\rangle + \sqrt{m} |\uparrow\rangle_s |m_e\rangle)$, where the three components of $|\psi_m^1\rangle$ represent the photon in the cavity, the excited source atom, and the absorption of the photon by the ensemble, respectively. The state $|\psi_m^1\rangle$ has a decay rate $\kappa_m \equiv \kappa + (m+1)\frac{g^2}{\Delta^2}\Gamma$ due to both the cavity decay (κ) and scattering from the admixed atomic excited states (Γ_e) of the source and the m atoms of the target ensemble, where any decay of $|\psi_m^1\rangle$ would leave s in $|\uparrow\rangle_s$.

Then, turning on a single weak tone $\Omega > 0$ with a detuning δ matching the energy of $|\psi_m^1\rangle$ perturbatively couples $|\psi_m^0\rangle$ to $|\psi_m^1\rangle$ with strength $w \equiv \langle\psi_m^1| \Omega |e\rangle_s \, {}_s\langle\downarrow| |\psi_m^0\rangle = \Omega g/\Delta$. We can then write an effective Hamiltonian in terms of the dressed states,

$$H = \sum_{m=0}^{N} \big[-\delta \, |\psi_m^0\rangle\langle\psi_m^0| - (m+1)d \, |\psi_m^1\rangle\langle\psi_m^1| + w \, |\psi_m^1\rangle\langle\psi_m^0| + \text{H.c.}\big]. \tag{3}$$

Here, w couples $|\psi_m^0\rangle$ to state $|\psi_m^1\rangle$, via which it decays into the continuum at a rate [37]

$$\Gamma_m = \frac{w^2}{(\kappa_m/2)^2 + (\delta - (m+1)d)^2} \kappa_m. \tag{4}$$

We denote the quasicontinuum state that $|\psi_m^0\rangle$ decays into as $|0\rangle_c |\uparrow\rangle_s |L_m(t)\rangle$, with $|L_m(t)\rangle$ a superposition across states of the ensemble and modes of the environment E, with the photon having leaked out of the cavity or having been scattered by an atom. The initial state with the ensemble in $|m\rangle$ and the environment in the vacuum decays toward this quasicontinuum of scattered photon states, evolving as [38,39]

$$e^{-\Gamma_m t/2} |0\rangle_c |\downarrow\rangle_s |m\rangle |\text{vac}\rangle_E + \sqrt{1 - e^{-\Gamma_m t}} \, |0\rangle_c |\uparrow\rangle_s |L_m(t)\rangle , \tag{5}$$

where we neglect, for now, any additional overall phase on the first term due to a Stark shift.

We illustrate the carving procedure by first considering a superposition $\frac{1}{\sqrt{2}}(|n\rangle + |n+1\rangle)$ of just two neighboring Dicke states spaced by d in energy. Here, $|n+1\rangle$ denotes the Dicke state which we wish to retain after carving, and $|n\rangle$ the state that we strive to annihilate.

To annihilate $|n\rangle$, we tune the coupling laser Ω to resonance with the dressed state energy, $\delta = -(n+1)d$, so that $|n\rangle$ decays at rate $\Gamma_n = 4w^2/\kappa_n$. Ω also addresses $|n+1\rangle$, but off resonantly by d, resulting in a slower decay $\Gamma_{n+1} = \Gamma_n/[1 + (2d/\kappa_n)^2]$ (assuming $\kappa_{n+1} \approx \kappa_n$ for an optimally chosen value of Δ, as explained below). The components $|n\rangle$, $|n+1\rangle$ then evolve according to Eq. (5), so that postselecting counterfactually on measuring the source atom after time t to have remained in the state $|\downarrow\rangle_s$ projects the system to the (not normalized) state

$$|\downarrow\rangle_s (e^{-\Gamma_n t/2} |n\rangle + e^{-\Gamma_{n+1} t/2} |n+1\rangle). \tag{6}$$

Choosing $t = 1/\Gamma_{n+1}$, the population of $|n+1\rangle$ decays only by a factor e^{-1}, and we maintain an order-unity success probability of $e^{-1}/2$, while the population of $|n\rangle$ is suppressed exponentially by a factor $e^{-\Gamma_n/\Gamma_{n+1}} = e^{-(1+(2d/\kappa_n)^2)} \ll 1$ even for modestly large d/κ_n.

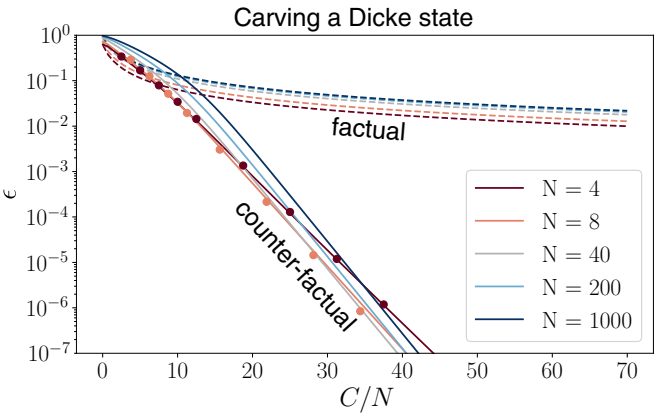

FIG. 3. Infidelity ϵ of carving Dicke states on the equator of the N-atom Bloch sphere. Analytical expressions for factual (dashed) [21] and counterfactual (solid) carving, analogous to Eqs. (9) and (7). For counterfactual carving, we drive with multiple tones as in Fig. 2 to annihilate all Dicke levels except $|m = N/2\rangle$. Solid dots are numerical simulations of counterfactual carving with the master equation, modeling the joint source-cavity-ensemble system for $N = 4$ and 8.

The suppression factor is maximized when $|n\rangle$ and $|n+1\rangle$ are maximally distinguishable, i.e., when the atomic detuning Δ is chosen such that losses between cavity and atomic decay are balanced, $\kappa = n\frac{g^2}{\Delta^2}\Gamma_e$, in which case $\kappa_n = 2\kappa$ (again, recall we take $\kappa \ll \Gamma_e$). The cooperativity C then determines the distinguishability since $d = \kappa\sqrt{C/n}$, making $4d^2/\kappa_n^2 = C/n$. The infidelity $\epsilon_{\rm cf}$ of the state from Eq. (6) with respect to $|n+1\rangle$ is then

$$\epsilon_{\rm cf} = \frac{e^{-C/n}}{1 + e^{-C/n}} \approx e^{-C/n}, \tag{7}$$

for $C/n \gg 1$. Note the dependence on the ratio C/n, where n enters since admixing the excited states of more target qubits further broadens the dressed state linewidth. This means we can more easily carve away adjacent levels around lower n, with $n = 1$ corresponding to a W state, and $n \sim N/2$ for carving states near the equator of the many-atom Bloch sphere, as in Fig. 2.

The results from Eq. (7) (and illustrated later in the results in Figs. 3 and 4) represent an exponential improvement in the scaling of the residual error ϵ compared to prior "factual" carving methods. In the setting we consider here with the source atom s, factual carving with a tone tuned to $|n\rangle$ would involve detecting a photon successfully exiting through the cavity mirror, thereby postselecting on $|\uparrow\rangle_s$ terms where the photon has leaked out of the cavity (as opposed to the $|\downarrow\rangle_s$ terms for counterfactual carving) from Eq. (5). We can approximate the terms remaining after postselection from Eq. (5) for small t, at which point the carving will be of the highest fidelity,

$$\sqrt{1 - e^{-\Gamma_n t}} \, |n\rangle + \sqrt{1 - e^{-\Gamma_{n+1} t}} \, |n+1\rangle \approx \sqrt{\Gamma_n t} \, |n\rangle + \sqrt{\Gamma_{n+1} t} \, |n+1\rangle . \tag{8}$$

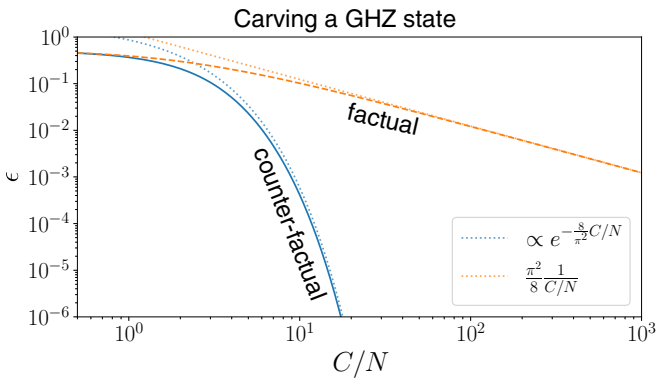

FIG. 4. Analytical expressions showing GHZ state infidelity for counterfactual [blue, Eq. (13)] and factual (yellow, Supplemental Material [36]) methods. Dotted lines indicate asymptotic analytical expressions valid for $C/N \gg 1$.

Because factual carving actively drives both $|n\rangle$ and $|n+1\rangle$ toward states with an expelled photon, we can only achieve population distortions proportional to the rates. The infidelity $\epsilon_{\rm f}$ for the factual method when attempting to create the state $|n\rangle$ is then

$$\epsilon_{\rm f} = \frac{\Gamma_{n+1}}{\Gamma_n + \Gamma_{n+1}} = \frac{1}{2 + C/n} \xrightarrow[\frac{C}{n}\gg 1]{} \frac{1}{C/n}. \tag{9}$$

This result also holds for the photon transmission variant of factual carving [21] due to the polynomial tail of Lorentzian transmission line shape overlapping with neighboring Dicke states, with similar polynomial scaling for other coherent evolution methods [16] (see the Supplemental Material [36]).

A. Carving a single Dicke state

Having illustrated the principle of counterfactual carving with two neighboring levels $|n\rangle$, $|n+1\rangle$, in Fig. 3 we show results when counterfactually carving a highly entangled Dicke state $|m = N/2\rangle$ from an initial coherent spin state (CSS) along the equator of the Bloch sphere, for the same setup as in Fig. 2. The joint source-cavity-ensemble system is prepared in the pure state $|\downarrow\rangle_s |0\rangle_c |+\rangle^{\otimes N}$, where $|+\rangle \equiv (|\downarrow\rangle + |\uparrow\rangle)/\sqrt{2}$, and evolves under the total Hamiltonian with simultaneous driving of tones Ω applied to all levels except $|m = N/2\rangle$. Analytical expressions for the multiparticle infidelity ϵ are obtained by summing contributions Γ_m across all driving tones to determine the relative populations of the levels $|m\rangle$. Each data point (large dots) in Fig. 3 is obtained separately by a simulation of the master equation for the joint source-cavity-ensemble system as in Fig. 2(b), where the evolution time $t_{1/e}$ is chosen to be when the population of $|\downarrow\rangle_s$ has been reduced by a factor $1/e$. Then, to postselect on measuring no jump in the source atom's state, we project the density matrix of the full system, $\rho_{\rm tot}(t = t_{1/e})$, onto $|\downarrow\rangle_s$ and renormalize. Finally, we trace out the source atom and the cavity mode, leaving just the reduced density matrix of the ensemble, $\rho_{\rm ensemble}(t = t_{1/e})$, computing its infidelity compared to the Dicke state at the equator $|m = N/2\rangle$, $\epsilon = 1 - \langle m = N/2| \rho_{\rm ensemble}(t = t_{1/e}) |m = N/2\rangle$. Fitting the asymptotic behavior, for $N = 8$ we have $\epsilon_{\rm cf} \approx 1.9 \times e^{-0.41C/N}$. Also shown in Fig. 3 is the fidelity for carving a Dicke state factually as in [21] using a tone tuned directly to $|m = N/2\rangle$. The corresponding success probabilities are $|c_{N/2}|^2 \approx 1/\sqrt{N}$ due to the population overlap of the initial CSS with $|m = N/2\rangle$, times factors of $1/e$ for counterfactual (for our chosen evolution time $t_{1/e}$) and $1/4$ for factual carving (due to photon transmission probability; see the Supplemental Material [36] and Ref. [21]).

B. Carving a GHZ state

In addition to carving individual nonclassical Dicke states, it is also possible to counterfactually carve a superposition of Dicke levels and generate other entangled states, including GHZ states. We can carve a GHZ state, $|{\rm GHZ}\rangle = \frac{1}{\sqrt{2}}(|+\rangle^{\otimes N} + |-\rangle^{\otimes N})$, by removing all the $|m\rangle$ with m odd from the CSS $|+\rangle^{\otimes N}$. One can see this equality since the components with an odd number of qubits in $|\downarrow\rangle$ cancel when expanding the above expression for $|{\rm GHZ}\rangle$. For large N, $|+\rangle^{\otimes N}$ is a superposition of Dicke states near the equator of the Bloch sphere, with $m \sim N/2$, where the Lorentzians have a (here approximated to be identical) width $\kappa_m \sim 2\kappa$. To remove the odd-m states via counterfactual carving, we apply a resonant tone to each and, for simplicity, we imagine an infinite ladder of such tones resonant with the odd m.

Turning on this ladder of tones resonant with the odd-m levels, each level sees no net phase shift, and recalling Eq. (4), each level m now decays with a total decay rate $\Gamma_m^{\rm tot}$ due to contributions from multiple driving tones Ω, with distinct values $\Gamma_{\rm even}^{\rm tot}$ and $\Gamma_{\rm odd}^{\rm tot}$ for even and odd m. The odd levels decay at a rate given by the resonant tone and by off-resonant tones above and below in energy detuned by multiples of $2d$, with $d = \kappa\sqrt{C/m}$ when optimized with $m \sim N/2$. Letting $\Gamma_{\rm res} \equiv \frac{2w^2}{\kappa}$ be the decay rate due to a resonant tone, the total decay rate for an odd level is then the sum of the contribution of the resonant tone directly addressing it, and a smaller contribution from all the of resonant tones as well, which we can sum as

$$\Gamma_{\rm odd}^{\rm tot} = \Gamma_{\rm res} + \Gamma_{\rm res} 2\sum_{j=1}^{\infty} \frac{1}{1 + (2j)^2 C/(N/2)}$$
$$\xrightarrow[\frac{C}{N}\gg 1]{} \Gamma_{\rm res}\left(1 + \frac{\pi^2}{24}\frac{1}{C/N}\right). \tag{10}$$

Similarly, the even m, which we wish to preserve, are addressed only off resonantly by tones above and below detuned by a distance of $d, 3d, 5d, \ldots$, which we can also sum over to give the overall rate that they decay:

$$\Gamma_{\rm even}^{\rm tot} = \Gamma_{\rm res} 2\sum_{j} \frac{1}{1 + (2j-1)^2 C/(N/2)} \xrightarrow[\frac{C}{N}\gg 1]{} \Gamma_{\rm res}\frac{\pi^2}{8}\frac{1}{C/N}. \tag{11}$$

For large C/N, the levels with odd m decay at a rate primarily determined by just the tone that directly addresses them, while the decay rate of the levels with even m is suppressed polynomially in C/N. With these two distinct values for the decay rates of the even- and odd-m levels, we can separate our initial CSS state into even and odd

components, with $|\text{even } m\rangle \equiv \frac{1}{\sqrt{2}}(|+\rangle^{\otimes N} + |-\rangle^{\otimes N})$ and $|\text{odd } m\rangle \equiv \frac{1}{\sqrt{2}}(|+\rangle^{\otimes N} - |-\rangle^{\otimes N})$, which then evolve similarly to Eq. (5) as

$$\begin{aligned}|+\rangle^{\otimes N} &= \frac{1}{\sqrt{2}}(|\text{even } m\rangle + |\text{odd } m\rangle) \\ &\to \frac{1}{\sqrt{2}}\left(e^{-\Gamma^{\text{tot}}_{\text{even}} t/2}\,|\text{even } m\rangle + e^{-\Gamma^{\text{tot}}_{\text{odd}} t/2}\,|\text{odd } m\rangle\right) \\ &\quad + \text{ photon-scattering terms}, \end{aligned} \tag{12}$$

where we have made $\Gamma^{\text{tot}}_{\text{odd}} > \Gamma^{\text{tot}}_{\text{even}}$ by tuning laser tones into resonance with the odd m.

To carve the GHZ state $|\text{even } m\rangle$ counterfactually, we choose $t = 1/\Gamma^{\text{tot}}_{\text{even}}$ so that the even levels will have decayed by only an amount $1/e$, guaranteeing a success probability of at least $\frac{1}{2}\frac{1}{e}$. Postselecting on the terms from Eq. (12) with no photon scattering, we have $\epsilon_{\text{cf}} = e^{-\Gamma^{\text{tot}}_{\text{odd}} t}/(e^{-\Gamma^{\text{tot}}_{\text{odd}} t} + e^{-\Gamma^{\text{tot}}_{\text{even}} t})$. The residual error is then

$$\epsilon_{\text{cf}} = \frac{e^{-\Gamma^{\text{tot}}_{\text{odd}}/\Gamma^{\text{tot}}_{\text{even}}}}{e^{-\Gamma^{\text{tot}}_{\text{odd}}/\Gamma^{\text{tot}}_{\text{even}}} + e^{-1}} \xrightarrow[\frac{C}{N}\gg 1]{} e e^{-\Gamma^{\text{tot}}_{\text{odd}}/\Gamma^{\text{tot}}_{\text{even}}} = e^{\frac{2}{3}} e^{-\frac{8}{\pi^2} C/N}. \tag{13}$$

Similarly, one can also carve the same GHZ state factually with a ladder of tones applied directly to the even levels, but here again, the polynomial spectral overlap of the shifted cavity resonances leads only to polynomial. suppression of the infidelity in C/N. In Fig. 4, we plot the residual error for factual and counterfactual carving, summing over contributions from all the tones (see the Supplemental Material [36] additional background about factual carving methods and the expressions for the sum over tones in this case). The result is the same asymptotic scaling as Eq. (7), just with a slightly different numerical coefficient, in this case $\epsilon_{\text{cf}} \approx e^{-\frac{C}{N}\frac{8}{\pi^2}}$ for counterfactual carving and, for comparison, $\epsilon_{\text{f}} \approx \frac{\pi^2}{8}\frac{1}{C/N}$ for the factual method. Note that the time t as well as C/N both scale as $\ln(1/\epsilon_{\text{cf}})$.

IV. CARVING PHASES ONTO ENTANGLED STATES

Counterfactual carving can alter not only the magnitude of an initial coefficient c_m, but also its phase, by detuning a drive Ω slightly from the energy of $|m\rangle$ to induce a Stark shift. One can then carve states with arbitrary phase,

$$\sum_m c_m |m\rangle \to \sum_m c_m e^{i\phi_m} e^{-\ell_m/2} |m\rangle . \tag{14}$$

Imprinting a phase ϕ_m as in Eq. (14) leads to small additional phase shifts and amplitude decays on adjacent levels, but these disturbances are efficiently correctable with compensating tones (see the Supplemental Material [36] for an iterative method to do this). With the ability to control both amplitudes and phases of different Dicke states, we now have access to a toolbox for carving high-fidelity multiparticle states while requiring only moderate cooperativity C.

V. PROSPECTS FOR EXPERIMENTAL IMPLEMENTATIONS

Recently, several groups have integrated cavities with single-atom arrays, enabling exquisite control of individual atoms coupled to an optical mode [40–46]. This presents a promising platform for realizing counterfactual carving and provides motivation for continued cooperativity improvements, as even modest improvements lead to large gains in achievable fidelity. For example, from the results in Fig. 4, with the cooperativity achieved in Ref. [47], using ^{87}Rb one could counterfactually carve GHZ states with $N \sim 10$ atoms with $\lesssim 10^{-4}$ infidelity. Such states can be transformed into "star" resource states [13,14], forming the basis of a neutral-atom measurement-based quantum computer with a cooperativity-dependent error contribution 100 times below thresholds for error-correcting codes [15]. Achieving the same fidelity with factual carving would require a cavity of cooperativity $\sim 10^5$, which is many orders of magnitude larger.

VI. CONCLUSION

In addition to achieving exponentially better fidelity, counterfactual carving is of fundamental interest as it harnesses the "no-jump" [28,29] evolution of a probe coupled to a qubit ensemble to exploit a curious property of quantum measurements, i.e., how merely giving the probe the possibility to evolve is sufficient to alter the quantum state even in instances where no probe evolution is observed.

While in the above analysis, for the sake of definiteness, we have applied counterfactual carving in the setting of cavity QED, relating it to the most pertinent prior works [21,22], counterfactual carving is a general approach applicable to many quantum systems. In the Supplemental Material [36], we have included a more general treatment.

ACKNOWLEDGMENTS

This project was funded in part by DARPA under the ONISQ program (Grant No. 134371-5113608), the MIT-Harvard Center for Ultracold Atoms (NSF Grant No. PHY-1734011), Quera, and the ARO (Grant No. W911NF1910517). Support is also acknowledged from the U.S. Department of Energy, Office of Science, National Quantum Information Science Research Centers, Quantum Systems Accelerator (Contract No. 7571809).

J.R. invented the counterfactual carving method, worked out the scaling properties, and drafted the manuscript. J.R. and J.S. together conceptually developed the work and the intuitive understanding of carving presented in this manuscript. Z.L. performed the analysis and numerical simulations of the one-axis twisting evolution presented in the Supplemental Material [36]. V.V. supervised the project. All authors discussed the method and results, and contributed to the manuscript.

[1] M. Kitagawa and M. Ueda, Squeezed spin states, Phys. Rev. A **47**, 5138 (1993).

[2] L.-M. Duan, M. D. Lukin, J. I. Cirac, and P. Zoller, Long-distance quantum communication with atomic

ensembles and linear optics, Nature (London) **414**, 413 (2001).
[3] B. M. Terhal, Quantum error correction for quantum memories, Rev. Mod. Phys. **87**, 307 (2015).
[4] R. Raussendorf and H. J. Briegel, A one-way quantum computer, Phys. Rev. Lett. **86**, 5188 (2001).
[5] R. Raussendorf, D. E. Browne, and H. J. Briegel, Measurement-based quantum computation on cluster states, Phys. Rev. A **68**, 022312 (2003).
[6] L.-M. Duan, B. Wang, and H. J. Kimble, Robust quantum gates on neutral atoms with cavity-assisted photon scattering, Phys. Rev. A **72**, 032333 (2005).
[7] E. M. Kessler, P. Kómár, M. Bishof, L. Jiang, A. S. Sørensen, J. Ye, and M. D. Lukin, Heisenberg-limited atom clocks based on entangled qubits, Phys. Rev. Lett. **112**, 190403 (2014).
[8] J. M. Robinson, M. Miklos, Y. M. Tso, C. J. Kennedy, T. Bothwell, D. Kedar, J. K. Thompson, and J. Ye, Direct comparison of two spin-squeezed optical clock ensembles at the 10 level, Nat. Phys. **20**, 208 (2024).
[9] B. K. Malia, Y. Wu, J. Martínez-Rincón, and M. A. Kasevich, Distributed quantum sensing with mode-entangled spin-squeezed atomic states, Nature (London) **612**, 661 (2022).
[10] A. Sondberg Sørensen and K. Mølmer, Entangling atoms in bad cavities, Phys. Rev. A **66**, 022314 (2002).
[11] J. Ramette, J. Sinclair, Z. Vendeiro, A. Rudelis, M. Cetina, and V. Vuletić, Any-to-any connected cavity-mediated architecture for quantum computing with trapped ions or Rydberg arrays, PRX Quantum **3**, 010344 (2022).
[12] A. Reiserer and G. Rempe, Cavity-based quantum networks with single atoms and optical photons, Rev. Mod. Phys. **87**, 1379 (2015).
[13] M. Hein, W. Dür, J. Eisert, R. Raussendorf, M. V. den Nest, and H. J. Briegel, Entanglement in graph states and its applications, arXiv:quant-ph/0602096.
[14] Y. Li, P. C. Humphreys, G. J. Mendoza, and S. C. Benjamin, Resource costs for fault-tolerant linear optical quantum computing, Phys. Rev. X **5**, 041007 (2015).
[15] R. Raussendorf, J. Harrington, and K. Goyal, Topological fault-tolerance in cluster state quantum computation, New J. Phys. **9**, 199 (2007).
[16] Z. Li, B. Braverman, S. Colombo, C. Shu, A. Kawasaki, A. F. Adiyatullin, E. Pedrozo-Peñafiel, E. Mendez, and V. Vuletić, Collective spin-light and light-mediated spin-spin interactions in an optical cavity, PRX Quantum **3**, 020308 (2022).
[17] Y. Zhao, R. Zhang, W. Chen, X.-B. Wang, and J. Hu, Creation of Greenberger-Horne-Zeilinger states with thousands of atoms by entanglement amplification, npj Quantum Inf. **7**, 24 (2021).
[18] T. Zhang, Z. Chi, and J. Hu, Entanglement generation via single-qubit rotations in a teared Hilbert space, PRX Quantum **5**, 030345 (2024).
[19] J. Von Neumann, *Mathematical Foundations of Quantum Mechanics* (Princeton University Press, Princeton, NJ, 1955).
[20] J. Borregaard, P. Kómár, E. M. Kessler, A. S. Sørensen, and M. D. Lukin, Heralded quantum gates with integrated error detection in optical cavities, Phys. Rev. Lett. **114**, 110502 (2015).
[21] W. Chen, J. Hu, Y. Duan, B. Braverman, H. Zhang, and V. Vuletić, Carving complex many-atom entangled states by single-photon detection, Phys. Rev. Lett. **115**, 250502 (2015).
[22] E. J. Davis, Z. Wang, A. H. Safavi-Naeini, and M. H. Schleier-Smith, Painting nonclassical states of spin or motion with shaped single photons, Phys. Rev. Lett. **121**, 123602 (2018).
[23] S. Welte, B. Hacker, S. Daiss, S. Ritter, and G. Rempe, Cavity carving of atomic Bell states, Phys. Rev. Lett. **118**, 210503 (2017).
[24] T. Đorđević, P. Samutpraphoot, P. L. Ocola, H. Bernien, B. Grinkemeyer, I. Dimitrova, V. Vuletić, and M. D. Lukin, Entanglement transport and a nanophotonic interface for atoms in optical tweezers, Science **373**, 1511 (2021).
[25] R. H. Dicke, Coherence in spontaneous radiation processes, Phys. Rev. **93**, 99 (1954).
[26] R. McConnell, H. Zhang, J. Hu, S. Cuk, and V. Vuletić, Entanglement with negative Wigner function of almost 3000 atoms heralded by one photon, Nature (London) **519**, 439 (2015).
[27] H. Tanji-Suzuki, I. D. Leroux, M. H. Schleier-Smith, M. Cetina, A. T. Grier, J. Simon, and V. Vuletic, Interaction between atomic ensembles and optical resonators: Classical description, Adv. At. Mol. Opt. Phys. **60**, 201 (2011).
[28] H. Carmichael, *An open systems approach to quantum optics: Lectures presented at the Université Libre de Bruxelles, October 28 to November 4, 1991*, Lecture Notes in Physics, New Series M, Monographs Vol. 18 (Springer, Berlin, 1993).
[29] A. Steinberg, Quantum measurements: A modern view for quantum optics experimentalists, arXiv:1406.5535.
[30] A. Omran, H. Levine, A. Keesling, G. Semeghini, T. T. Wang, S. Ebadi, H. Bernien, A. S. Zibrov, H. Pichler, S. Choi, J. Cui, M. Rossignolo, P. Rembold, S. Montangero, T. Calarco, M. Endres, M. Greiner, V. Vuletić, and M. D. Lukin, Generation and manipulation of Schrödinger cat states in Rydberg atom arrays, Science **365**, 570 (2019).
[31] C. Song, K. Xu, H. Li, Y.-R. Zhang, X. Zhang, W. Liu, Q. Guo, Z. Wang, W. Ren, J. Hao, H. Feng, H. Fan, D. Zheng, D.-W. Wang, H. Wang, and S.-Y. Zhu, Generation of multicomponent atomic Schrödinger cat states of up to 20 qubits, Science **365**, 574 (2019).
[32] S. A. Moses *et al.*, A race-track trapped-ion quantum processor, Phys. Rev. X **13**, 041052 (2023).
[33] C. L. Degen, F. Reinhard, and P. Cappellaro, Quantum sensing, Rev. Mod. Phys. **89**, 035002 (2017).
[34] L. Pezzè, A. Smerzi, M. K. Oberthaler, R. Schmied, and P. Treutlein, Quantum metrology with nonclassical states of atomic ensembles, Rev. Mod. Phys. **90**, 035005 (2018).
[35] H. J. Kimble, Strong interactions of single atoms and photons in cavity QED, Phys. Scr. **1998**, 127 (1998).
[36] See Supplemental Material at http://link.aps.org/supplemental/10.1103/PhysRevA.111.052426 for a general model of counter-factual carving which applies beyond cavity QED, a comparison of the scaling of the fidelity achievable for generating GHZ states from counter-factual carving vs cavity-driven coherent evolution techniques, and a procedure for carving both amplitudes and phases.
[37] C. Cohen-Tannoudji, J. Dupont-Roc, and G. Grynberg, *Atom-Photon Interactions* (Wiley, New York, 1998).
[38] M. O. Scully and M. S. Zubairy, *Quantum Optics* (Cambridge University Press, Cambridge, 1997).
[39] M. D. Lukin, *Modern Atomic and Optical Physics II Lecture Notes* (2016).
[40] Z. Yan, J. Ho, Y.-H. Lu, S. J. Masson, A. Asenjo-Garcia, and D. M. Stamper-Kurn, Superradiant and subradiant

cavity scattering by atom arrays, Phys. Rev. Lett. **131**, 253603 (2023).

[41] H. R. Kong, J. Taylor, Y. Dong, and K. S. Choi, Melting a Rydberg ice to a topological spin liquid with cavity vacuum fluctuation arXiv:2109.03741.

[42] H. R. Kong and K. S. Choi, Physical limits of ultra-high-finesse optical cavities: Taming two-level systems of glassy metal oxides, arXiv:2109.01856.

[43] Y. Liu, Z. Wang, P. Yang, Q. Wang, Q. Fan, S. Guan, G. Li, P. Zhang, and T. Zhang, Realization of strong coupling between deterministic single-atom arrays and a high-finesse miniature optical cavity, Phys. Rev. Lett. **130**, 173601 (2023).

[44] Y.-T. Chen, M. Szurek, B. Hu, J. de Hond, B. Braverman, and V. Vuletic, High finesse bow-tie cavity for strong atom-photon coupling in Rydberg arrays, Opt. Express **30**, 37426 (2022).

[45] A. Rudelis, A cavity-coupled Rydberg atom array platform for quantum computing, Ph.D. thesis, MIT, 2023.

[46] D. Shadmany, A. Kumar, A. Soper, L. Palm, C. Yin, H. Ando, B. Li, L. Taneja, M. Jaffe, D. Schuster, and J. Simon, Cavity QED in a high Na resonator, arXiv:2407.04784.

[47] Y. Colombe, T. Steinmetz, G. Dubois, F. Linke, D. Hunger, and J. Reichel, Strong atom-field coupling for Bose-Einstein condensates in an optical cavity on a chip, Nature (London) **450**, 272 (2007).